Hydrogen-Induced Amorphization in Intermetallic Compounds

Hydrogen-Induced Amorphization in Intermetallic Compounds*

Kiyoshi Aoki and Tsuyoshi Masumoto

Institute for Materials Research

(Received March 4, 1988)

Synopsis

This article briefly reviews our recent studies on the hydrogen-induced amorphization (HIA), i.e., the transformation from the crystalline to the amorphous state by hydrogen absorption, of the intermetallic compounds. The experimental evidence of amorphization, the amorphizing alloy systems, the progress and the mechanism of HIA, and the influence of HIA on the magnetic properties of the intermetallic compounds are described.

I. Introduction

Until recently the preparation of the amorphous alloys was confined to rapid quenching from the melt or vapor phases except for some special alloys prepared by an electroplating. For the formation of the amorphous alloys from the melt, the cooling rates higher than 10^4 K/s are required to suppress nucleation and growth of the more stable crystalline counterparts. This leads to severe dimensional and compositional restrictions in the production of amorphous alloys. For this reason, it is of considerable interest to explore the alternate process for the preparation of amorphous alloys. Recently, it was demonstrated that amorphous alloys can be prepared by a fundamentally different method, i.e., the solid state reaction. A pioneering example of this new approach is hydrogen-induced amorphization,i.e., the transformation from the crystalline to the amorphous state by hydrogen absorption, of the metastable Zr_3Rh alloy having the $L1_2$ structure(1). The HIA process of the Zr_3Al compound with the $L1_2$ structure was observed by high voltage transmission electron microscopy(2). The authors investigated the structural changes of many intermetallic compounds during the hydrogen absorption

---

* The 1831th report of Institute for Materials Research

process and demonstrated that HIA occurs in the compounds with the C15, C23, $D0_{19}$ and $L1_2$ structures(3-10). They followed the progress of HIA in the Laves phase $CeFe_2$ by TEM and magnetic property measurements and discussed the mechanism of HIA(11). Further, they investigated the structures (12) and magnetic properties of the amorphous alloys synthesized by hydrogen absorption(11,13,14). Although it has been suggested that amorphous alloys can be formed during the hydrogen absorption process(15-18), the actual experimetal results on HIA are limited to the above alloys. In the present article the amorphizing alloy systems, the progress of amorphization, magnetic properties of the amorphous alloys synthesized by hydrogenation are described and the mechanism of amorphization are discussed.

II. Experimental

The A_xB_{1-x} compounds (A = a rare earth metal and Zr, B = Fe, Co, Ni, Rh, Al, Ga, In) were prepared by arc melting in an argon atmosphere. Pulverized samples(under 100 mesh) were reacted with hydrogen(7N) below 5MPa of pressure between 293-773 K for 86.4 ks. The structures of the samples before and after hydrogenation were examined by powder XRD (monochromated CuK_α radiation). Some samples were further examined by transmission electron microscopy(TEM). The crystallization temperature was determined by differential scanning calorimetry (DSC) in a pure argon gas at a heating rate of 40 K/min. The magnetic properties of the samples were measured from 77 to 900 K by using a magnetic balance in an 8 kOe magnetic field.

III. Results and discussion

1. Formation of the amorphous alloys by hydrogen absorption

It has been reported that Bragg peaks in the XRD pattern disappear and are replaced by a broad maximum by hydrogenation of some R-M compounds (R: rare earth metal, M: 3d transition metal) (15)-(18). However, the simple observation of the XRD pattern is insufficient to distinguish amorphization from the disintegration into ultra fine powders. The authors have investigated the structural changes of the intermetallic compounds during the hydrogen absorption process by x-ray diffraction (XRD), transmission electron microscopy(TEM)and differential scanning calorimetry (DSC). Although

a large number of experiments were carried out using various alloys, we highlight the results obtained in the Laves phase $GdFe_2$ compound in this paper.

The change of XRD patterns of the Laves phase $GdFe_2$ compounds hydrogenated at various temperatures is shown in Figure 1 (12). $GdFe_2$ absorbs hydrogen without any change in the structure at 373 K, although the position of the Bragg peaks shifts to the lower angle side indicating the volume expansion of the crystal. In the XRD patterns of the samples hydrogenated at 473 K, however, the Bragg peaks disappear and are replaced by a broad maximum. On hydrogenation at 773 K, new Bragg peaks corresponding to GdH_2 and α-Fe appear. The samples showing the broad maximum in the XRD patterns were further examined by TEM. One observes the featureless microstructure in the bright field image (Figure 2a) and the diffuse halo characteristic of the amorphous phase in the diffraction pattern(Figure 2b). The lack of contrast in the micrograph and the presence of the halo in the diffraction pattern confirm the amorphous nature of the sample.

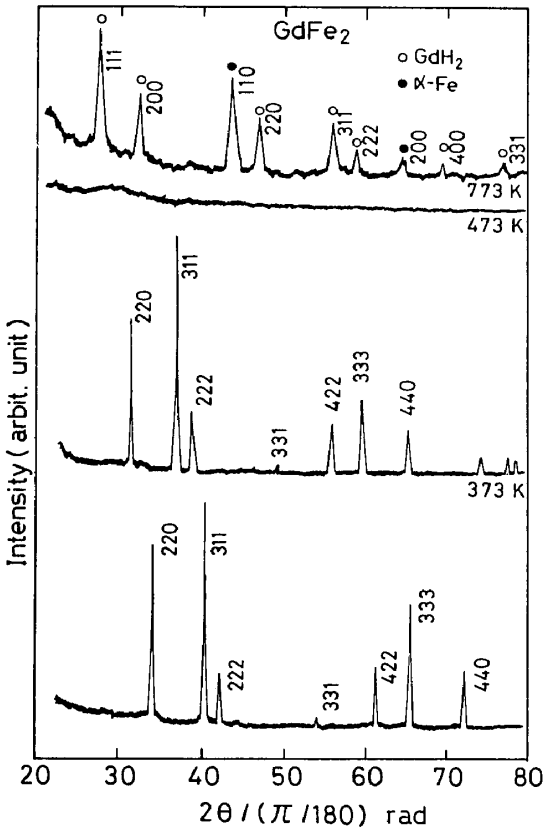

Figure 1 X-ray diffraction patterns of the $GdFe_2$ compound hydrogenated at various temperatures.

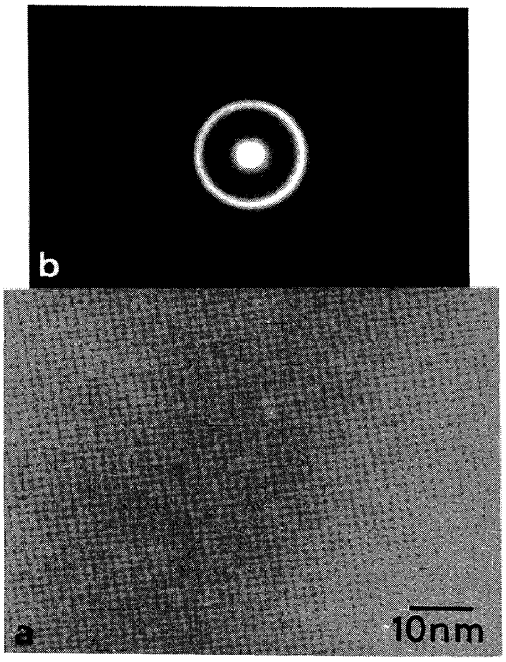

Figure 2 A transmission electron micrograph (a) and the corresponding diffraction pattern (b) of the $GdFe_2$ compound hydrogenated at 473 K.

The DSC curve of the above sample shows a broad endothermic peak resulting from partial desorption of hydrogen and two crystallization exothermic peaks as seen in Figure 3. Further, the amorphous nature of the hydrogen-induced amorphous a-$GdFe_2H_x$ alloy was established by the x-ray structural analysis (11). From XRD, TEM and DSC measurements, it is concluded that $GdFe_2$ transforms to the amorphous state around 500 K. Thus, hydrogenation of $GdFe_2$ gives rise to the formation of crystalline c-$GdFe_2H_x$, amorphous a-$FdFe_2H_x$, and GdH_2 and α-Fe with increasing temperature.

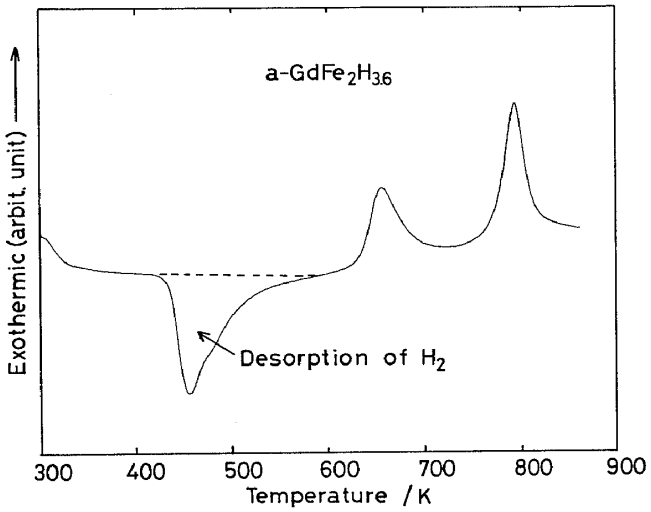

Figure 3 A DSC curve of a-$GdFe_2H_x$ synthesized by hydrogenation.

The structures of the Laves phase RFe_2(C15) compounds hydrogenated at various temperatures are tabulated in Table 1 (7). The crystallization temperature T_x of the amorphous alloy is also listed in the brackets. Of the eight RFe_2 compounds investigated in the present work, seven compounds ,i.e., YFe_2, $SmFe_2$, $GdFe_2$, $TbFe_2$, $DyFe_2$, $HoFe_2$ and $ErFe_2$, absorb hydrogen in the crystalline state below 450 K, amorphize between 450 and 550 K, and decompose into RH_2 and α-Fe above 550 K. Only $CeFe_2$ amorphizes below 450 K, and decomposes into CeH_2 and α-Fe above 550 K. It is worth noticing that all amorphous alloys are formed at the temperature range where the decomposition of the compounds is suppressed.

Table 2 and 3 show the amorphous alloys synthesized by hydrogenation of AB_2, A_3B and A_2B type intermetallic compounds, respectively(5,7,9,10). The previously reported data on the alloys which amorphize by hydrogenation are also listed in Table 3 (1,2).

Table 1 Structures of Laves phase RFe_2 compounds(C15) hydrogenated at 323, 473 and 773 K (5MPa H_2, 86.4ks) and the crystallization temperature T_x of the hydrogen-induced amorphous alloys.

Alloy	Structures after hydrogenation 323 K	473 K, [T_x(K)]	773 K
YFe_2	c-YFe_2H_x	a-YFe_2H_x [639]	YH_2 + α-Fe
$CeFe_2$	a-$CeFe_2H_x$	a-$CeFe_2H_x$ [563]	CeH_2 + α-Fe
$SmFe_2$	c-$SmFe_2H_x$	a-$SmFe_2H_x$ [620]	SmH_2 + α-Fe
$GdFe_2$	c-$GdFe_2H_x$	a-$GdFe_2H_x$ [643]	GdH_2 + α-Fe
$TbFe_2$	c-$TbFe_2H_x$	a-$TbFe_2H_x$ [647]	TbH_2 + α-Fe
$DyFe_2$	c-$DyFe_2H_x$	a-$DyFe_2H_x$ [650]	DyH_2 + α-Fe
$HoFe_2$	c-$HoFe_2H_x$	a-$HoFe_2H_x$ [649]	HoH_2 + α-Fe
$ErFe_2$	c-$ErFe_2H_x$	a-$ErFe_2H_x$ [651]	ErH_2 + α-Fe

The RNi_2 compounds amorphize over a wide temperature range including room temperature, while the RFe_2 and the RCo_2 compounds absorbs hydrogen in the crystalline state at room temperature and amorphize between about 400 -500 K. Only CeM_2 (M = Fe,Co,Ni) compounds amorphize over a wide temperature range. In these compounds the amorphous alloys are formed at the temperature range where the decomposition of the compounds into elemental hydride RH_2 and α-Fe, β-Co or RNi_5. Therefore, it is considered that such decompositions are the key for HIA in the Laves phase compounds. Recently, it has been discovered that HIA occurs in many R-Al and R-In compounds, too. However, the conditions under which HIA occurs and the mechanism of HIA are still uncertain.

2. The progress of hydrogen-induced amorphization

The progress of HIA in $CeFe_2$ was followed by both XRD and magnetic property measurements(11). The change in the XRD pattern of $CeFe_2$ during the hydrogen absorption is shown in Figure 4. An increase in the hydrogen concentration (H/M) reduces the intensity of Bragg peaks, but does not change the position of the Bragg peaks. A broad maximum overlapped with the Bragg peaks appear at medium hydrogen concentrations (0.2-0.8 H/M). Bragg peaks disappear almost completely for the sample hydrogenated to 1.0(H/M). It is well known that hydrogen atoms expand the crystal lattice which shifts the Bragg peaks towards the lower angle side. However, no change of the Bragg

Table 2 Hydrogen-induced amorphization of the AB_2 type (C15 Laves phase RM_2) intermetallic compounds by hydrogen absorption at 323 and 473 K (5MPa H_2, 86.4ks).

	A = Y	La	Ce	Pr	Nd	Sm	Eu	Gd	Tb	Dy	Ho	Er
B = Fe	●		○			●		●	●	●	●	●
Co			○	●	●	●		●	●	●	●	●
Ni	○	○	○	○		○		○	○	○	○	●

○ HIA occurs at both 323 and 473 K.
● HIA occurs around 473 K.

Table 3 Hydrogen-induced amorphization of the A_3B, A_2B type intermetallic compounds by hydrogen absorption at 300 K, (5MPa H_2, 86.4 ks).

(i) $A_3B(L1_2$ or fcc)

	A = Zr	La	Ce	Nd	Sm	Pr
B = Rh	○*					
Al	○**					
In	○	○	○	○	○	○
Ga				○	○	

* Reference(1)
** Reference(2)

(ii) $A_3B(D0_{19})$

	A = La	Ce	Nd	Pr
B = Al	○	○	○	○

(iii) $A_2B(C23)$

	A = Y	Pr	Nd	Sm	Gd	Tb	Dy	Ho
B = Al	○	○	○	○	○	○	○	○

peak position was observed. This suggests that hydrogen atoms do not substantially dissolve in the crystalline phase. Therefore, it is suggested that a-$CeFe_2H_x$ coexist with c-$CeFe_2H_x$.

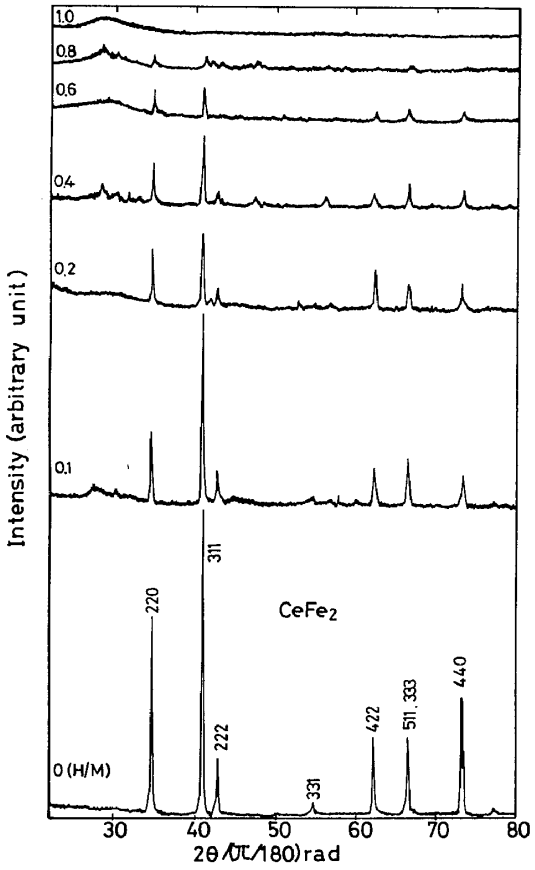

Figure 4 XRD patterns of the $CeFe_2$ samples as a function of hydrogen concentration.

The thermomagnetization curves of the samples containing hydrogen of 0.1-0.8 (H/M) show two stage decrements as seen in Figure 5. The first decrement is caused by the crystalline phase and the second gradual one is due to the amorphous phase. This suggests that the volume fraction of the latter increases gradually with increasing hydrogen concentration.

From these facts, we conclude that HIA starts locally and the regions of the amorphous phase spread gradually as shown schematically in Figure 6. The whole crystalline phase does not transform to the amorphous state, but a part of the crystalline phase changes to the amorphous phases and their region increases with the hydrogen concentration. Komatsu et al. observed by high voltage electron microscopy that the formation of the amorphous phase in Zr_3Al starts at lattice defects such as dislocations and grain boundaries(2). Similarly, HIA may start from such defects in the RM_2 compounds.

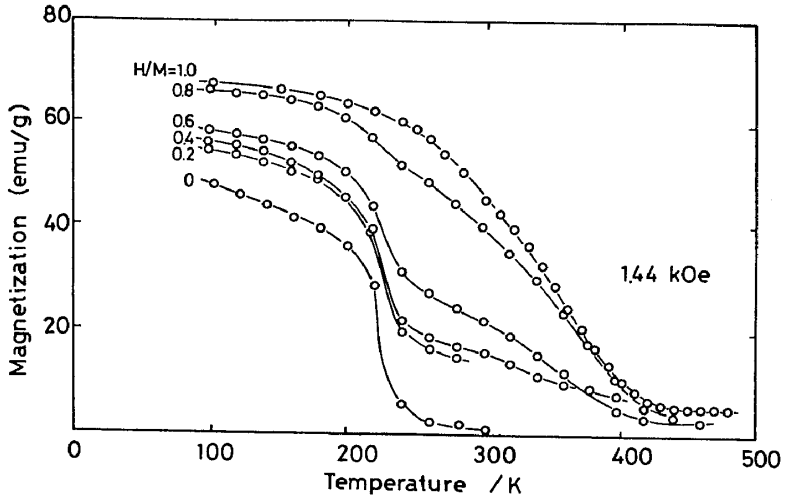

Figure 5 Thermomagnetization curves of the $CeFe_2$ samples with different hydrogen contents.

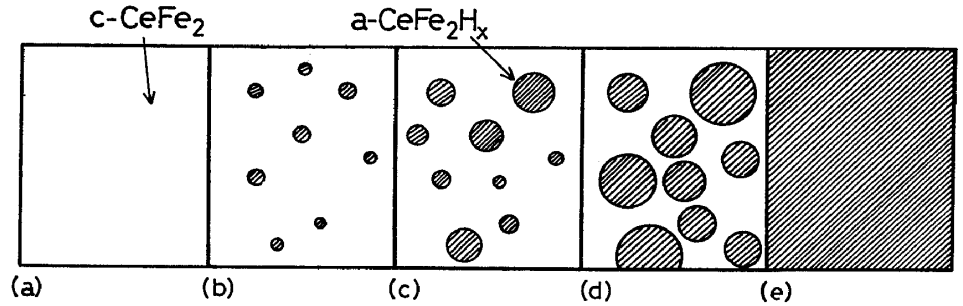

Figure 6 A schematic diagram of the progress of hydrogen-induced amorphization in the $CeFe_2$ compound.

3. The mechanism of hydrogen-induced amorphization in the Laves phase RM_2 compounds

In order for the HIA reaction to proceed, the amorphous phase must have a lower free energy than the corresponding crystalline product and a kinetic barrier must exist to prevent the formation of the equilibrium phases. The authors have recently observed by the differential thermal analysis (DTA) in a hydrogen atmosphere that the hydrogenated c-$GdFe_2H_x$ alloy transforms to a-$GdFe_2H_x$ exothermally around 470 K (19). This implies that a-$GdFe_2H_x$ is more stable rather than c-$GdFe_2H_x$, i.e., the free energy of the former is lower than that of the latter. This observation is a thermodynamic

ground for the occurrence of HIA. The mechanism of HIA in $GdFe_2$ is discussed with a help of the free energy.

Figure 7 (a)(b)(c) shows the hypothetical free energy diagram during the hydrogen absorption process in the $GdFe_2$ -H_2 system. Since mobility of Gd and Fe atoms is considerablly low at room temperature and thus rearrangement of metallic atoms is impossible, $GdFe_2$ absorbs hydrogen in the crystalline state. As we start hydrogenation, the composition moves along $GdFe_2$-H_2 axis as seen in Figure 7(a). If the free energy curve of a-$GdFe_2H_x$ lies above that of c-$GdFe_2H_x$, then it is impossible to have the HIA reaction. However, the free energy of the amorphous phase is lower than that of the crystalline phase as mentioned above. Therefore, the driving force for HIA exists. If the mobility of the metallic atoms become large so as to rearrange the local environmetal sites around hydrogen atoms, HIA occurs. In the present alloy this reaction occurs between 400 and 500 K. As we increase the temperature further, the amorphous phase is no more stable and the most stable phases GdH_2 and α -Fe are formed as seen in Figure 7(c)).

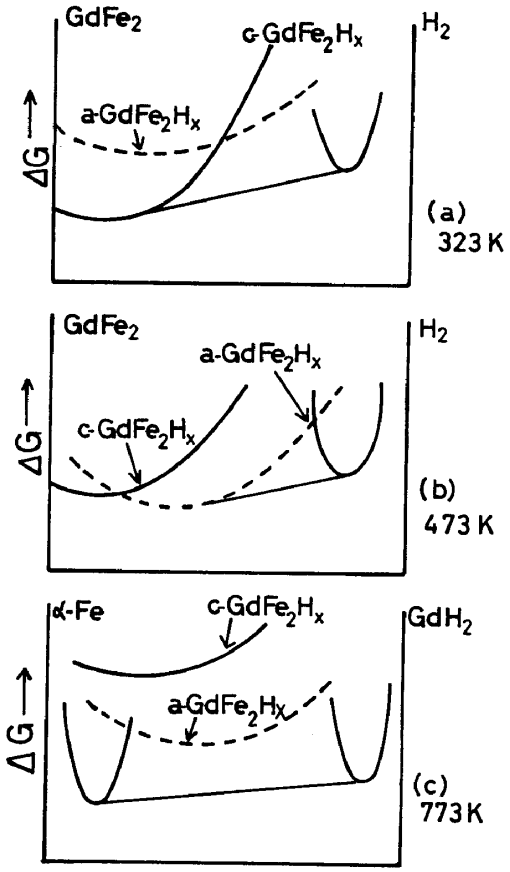

Figure 7 A hypothetical free energy diagram of the $GdFe_2$- H_2 system.

The differences of the free energy between a- and c-$GdFe_2H_x$ are discussed. Hydrogen atoms occupy the interstitial sites surrounded by 2Gd + 2Fe, 1Gd + 3Fe and 4Fe in c-$GdFe_2H_x$ by the geometrical constraint as shown schematically in Figure 8(a) (20). On the contrary, hydrogen atoms in the corresponding amorphous phase occupy tetrahedrally coordinated sites surrounded by 4Gd, 3Gd + 1Fe and 2Gd + 2Fe as shown in Figure 8(b). Such sites are energetically much more

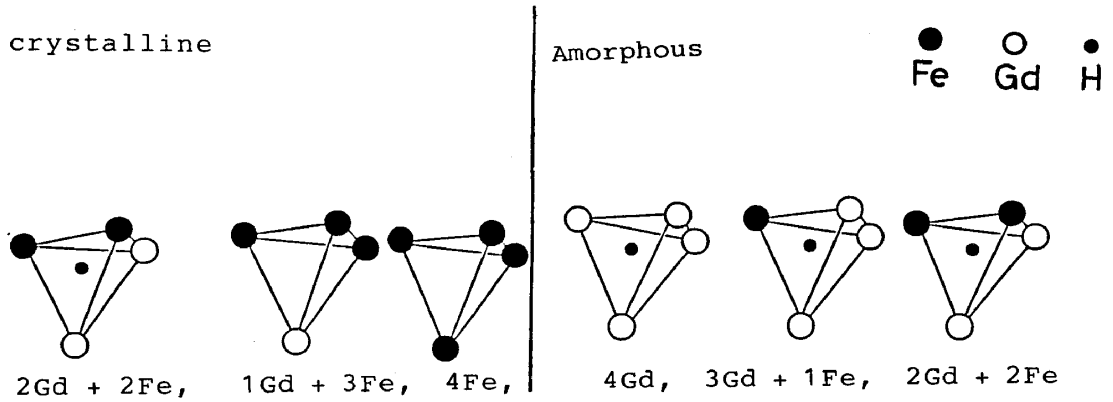

Figure 8 A schematic diagram of the hydrogen occupation sites for the c- and a-$GdFe_2H_x$ alloys.

favorable for the hydrogen occupancy. Thus, it is suggested that the thermodynamic driving force for HIA in $GdFe_2$ to be the enthalpy difference resulting from the different hydrogen occupation sites in both states of alloy.

4. Magnetic properties

Figure 9 shows the thermomagnetization curves of (1) the a-$Gd_{33}Fe_{67}$ prepared by rapid quenching, (2) the hydrogenated amorphous a-$Gd_{33}Fe_{67}H_{120}$, and (3) the a-$GdFe_2H_{3.6}$ synthesized by hydrogenation(12). The temperature dependence of the magnetization of the hydrogen-induced amorphous alloy is identical to that of the hydrogenated amorphous alloy. This suggests similarity of the structure of both amorphous alloys. As mentioned above, hydrogenation of $GdFe_2$ gives rise to the formation of c- and a-$GdFe_2H_x$, depending on the temperature. Of particular interest are the differences in the magnetic properties of them. The temperature dependence of the magnetization of a- and c-$GdFe_2H_x$ as well as the original compound c-$GdFe_2$ is shown in Figure 10. Hydrogen absorption is accopmanied by quite pronounced changes in the magnetic properties. It is noticeable that there is a pronounced differences between the thermomagnetization curves between a- and c-$GdFe_2H_x$. The magnetization of c-$GdFe_2H_x$ decreases drastically with increasing temperature around 100 K, but increases to the level of the original compound. The recovery of the magnetization results from desorption of hydrogen. The thermomagnetization curve of a-$GdFe_2H_{3.6}$ synthesized by hydrogenation

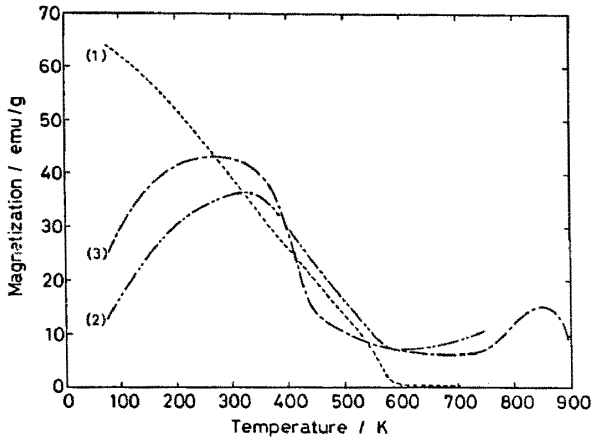

Figure 9 Thermomagnetization curves of the as-prepared amorphous alloy(1), the hydrogenated amorphous alloy(2), and the hydrogen-induced amorphous alloy in the $GdFe_2$ alloys.

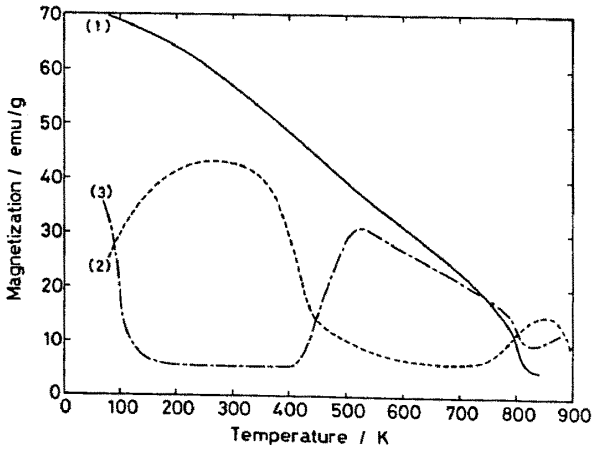

Figure 10 Thermomagnetization curves of the original compound(1), the hydrogen-induced amorphousalloy(2), and the hydrogenated crystalline alloy(3) in the $GdFe_2$ alloy.

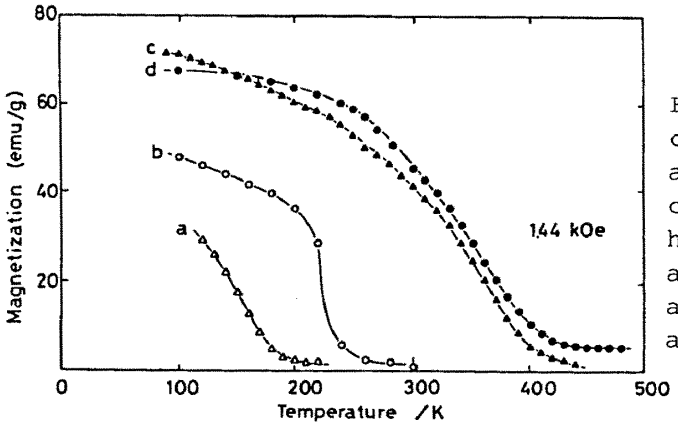

Figure 11 Thermomagnetization curves of the as-prepared amorphous alloy (a), the crystalline alloy (b), the hydrogenated amorphous alloy (c), and the hydrogen-induced amorphous alloy (d) in the $CeFe_2$ alloys.

Table 4 The Curie temperature of the hydrogen-induced amorphous RFe_2H_x.

	Tc(K)		Tc(K)
c-$CeFe_2$	265	c-$TbFe_2$	711
a-$CeFe_2H_x$(HIA)	410	a-$TbFe_2H_x$(HIA)	417
a-$Ce_{33}Fe_{67}$(SP)	265		
a-$Ce_{33}Fe_{67}H_x$(SP + H_2)	405		
		c-$DyFe_2$	635
c-$GdFe_2$	818	a-$DyFe_2H_x$(HIA)	426
c-$GdFe_2H_{4.4}$	107		
a-$GdFe_2H_{3.6}$(HIA)	443		
a-$Gd_{33}Fe_{67}$(RQ)	568	c-$HoFe_2$	612
a-$Gd_{33}Fe_{67}H_{120}$(RQ + H_2)	598	a-$HoFe_2H_x$(HIA)	412
		c-$ErFe_2$	578
		a-$ErFe_2H_x$(HIA)	409

HIA Hydrogen-induced amorphization
SP Sputtering
RQ Rapid quenching

shows two peaks around 300 and 850 K. From the XRD and DSC experiments it is concluded that the second peak results from the precipitation of α-Fe. The first peak of the thermomagnetization curve is not understood.

Figure 11 shows the thermomganetization of c-$CeFe_2$ and a-$Ce_{33}Fe_{67}$ film prepared by sputtering as well as the hydrogenated alloys. The magnetization of a- $Ce_{33}Fe_{67}$ is lower than that of the original compound c-$CeFe_2$. Hydrogen raises both the magnetization and the Curie temperature of the originally amorphous and crystalline alloy. The thermomagnetization curve of a-$CeFe_2H_3$ synthesized by hydrogenation is identical with that of the hydrogenated amorphous film within experimental accuracy. This supports the occurrence of HIA. The Curie temperature T_C of the $GdFe_2H_x$ alloys, determined from an Arrott plot of the thermomagnetization curves, are listed in Table 4. Absorption of hydrogen leads to sharp reduction in the Curie temperature of the crystalline alloy from 818 to 107 K, compared to the Curie temperature of 443 K for the HIA alloys. The Curie temperatures T_C of c-RFe_2 and a-RFe_2H_x (R = Ce, Gd, Tb, Dy, Ho and Er) synthesized by hydrogenation are listed in Table IV (10,12,13).

V. Summary and conclusions

The combination of the experimental results like the disappearance of the Bragg peaks, the appearance of the halos, the lack of the microstructures and the similarities of the magnetic properties with the amorphous phases produced by sputtering revealed the transition from the crystalline to the amorphous state by hydrogen absorption. The transformation is gradual and the region of the amorphous phase increases with increasing hydrogenation. The mechanism of the amorphization is closely related to the formation of the elemental hydride at the elevated temperatures.

Acknowledgements

The present work was suported in part by a Grant-In-Aid for the Scientific Research on Priority Areas, New Functionality Materials - Design, Preparation and Control, The Ministry of Education, Science and Culture (62504511).

References

(1) X. L. Yeh, K. Samwer and W. L. Johnson, Appl. Phys. Lett., **42**,(1983)242.

(2) M.Komatsu,H.Fujita and Y.Ishii, Collected Abst. Annual Meeting Japan Inst.Metals,(1984)209.

(3) K.Aoki, K.Shirakawa and T.Masumoto, Sci. Rep. RITU.,**A-32**, (1985)239.

(4) K.Aoki, T.Yamamoto and T.Masumoto, Sci. Rep. RITU., **A-33**, (1986)163.

(5) K. Aoki, T. Yamamoto and T. Masumoto, Scr.Metall.,**21**(1987)27.

(6) K.Chattopadhyay, K.Aoki and T.Masumoto, Scr.Metall, **21**(1987)163.

(7) K.Aoki,A.Yanagitani,X-G.Li and T.Masumoto, Mater.Sci.Eng., **89**(1988) in press.

(8) K.Aoki,X-G.Li and T.Masumoto, Scr.Metall, to be published.

(9) K.Aoki,X-G.Li, A.Yanagitani and T.Masumoto, 5th Japan Institute of Metals Int. Symposium on Non-equilibrium Solid Phases of Metals and Alloys, March 14-17,(1988),Kyoto, Japan.

(10) X-G.Li, K.Aoki and T.Masumoto, 5th Japan Institute of Metals Int. Symposium on Non-equilibrium Solid Phases of Metals and Alloys, March 14-17,(1988),Kyoto,Japan.

(11) K.Aoki,T.Yamamoto,Y.Satoh,K.Fukamichi and T.Masumoto, Acta Metall.,**35**,(1987)2465.

(12) E.Matsubara,Y.Ohzora,Y.Waseda,K.Aoki.K.Fukamichi and T.Masumoto, Z.Naturforsch,**42a**(1987)582.

(13) K.Aoki,M.Nagano,A.Yanagitani and T.Masumoto, J.Appy.Phys., **62**(1987)3314.

(14) A.Yanagitani,K.Aoki and T.Masumoto, 5th Japan Institute of Metals Int. Symposium on Non-equilibrium Solid Phases of of Metals and Alloys, March14-17,(1987), Kyoto, Japan.

(15) H. Oesterreicher, J. Clinton and H. Bittner, Mat. Res. Bull.,**11**(1976)1241.

(16) I. Jacob and D. Shaltiel, J. Less-Common Met., **65**(1979)117.

(17) K. H. J. Buschow, Solid State Commun.,**19**(1976)421.

(18) A. M. van Diepen and K. H. J. Buschow, Solid State Commun., **22**(1977)113.

(19) K.Aoki, A.Yanagitani and T.Masumoto, unpublished work.

(20) D. Ivey and D. Northwood, J. Less-common Met.,**115**(1986)23.